Protein chain collapse modulation and folding stimulation by GroEL-ES

Naqvi, Mohsin M.; Avellaneda, Mario J.; Roth, Andrew; Koers, Eline J.; Roland, Antoine; Sunderlikova, Vanda; Kramer, Günter; Rye, Hays S.; Tans, Sander J.

Important note
To cite this publication, please use the final published version (if applicable).
Please check the document version above.

BIOPHYSICS

Protein chain collapse modulation and folding stimulation by GroEL-ES

Mohsin M. Naqvi[1]†, Mario J. Avellaneda[1]‡, Andrew Roth[2], Eline J. Koers[1], Antoine Roland[1], Vanda Sunderlikova[1], Günter Kramer[3,4], Hays S. Rye[2], Sander J. Tans[1,5]*

The collapse of polypeptides is thought important to protein folding, aggregation, intrinsic disorder, and phase separation. However, whether polypeptide collapse is modulated in cells to control protein states is unclear. Here, using integrated protein manipulation and imaging, we show that the chaperonin GroEL-ES can accelerate the folding of proteins by strengthening their collapse. GroEL induces contractile forces in substrate chains, which draws them into the cavity and triggers a general compaction and discrete folding transitions, even for slow-folding proteins. This collapse enhancement is strongest in the nucleotide-bound states of GroEL and is aided by GroES binding to the cavity rim and by the amphiphilic C-terminal tails at the cavity bottom. Collapse modulation is distinct from other proposed GroEL-ES folding acceleration mechanisms, including steric confinement and misfold unfolding. Given the prevalence of collapse throughout the proteome, we conjecture that collapse modulation is more generally relevant within the protein quality control machinery.

INTRODUCTION

Unfolded proteins are thought to collapse autonomously into a compact yet dynamic state (*1*, *2*). This compaction is considered important to protein folding (*3*), aggregation (*4*, *5*), intrinsic disorder (*6*), and phase separation (*7*) and has been studied mainly for polypeptides that are free in solution (*8*–*10*). However, whether the collapse of protein chains can be controlled by other proteins including chaperones is poorly understood (*11*). GroEL-GroES is the archetypal protein-folding chaperone (*12*, *13*). Its folding mechanism has been studied extensively in experiments and theory (*14*–*18*). Unfolded substrates are thought to initially bind the apical domains at the rim of a GroEL ring, which is followed by adenosine 5′-triphosphate (ATP) and GroES binding, displacing the substrate protein into the enclosed GroEL-ES cavity and initiating folding, while ATP hydrolysis triggers cavity disassembly and release of GroES and substrate into free solution (*14*, *15*, *19*). However, a consensus on the core mechanism by which GroEL-ES stimulates protein folding is lacking. GroEL-ES has been proposed to accelerate folding directly, by sterically confining the unfolded substrates within its closed chamber, which can lower their entropy and thus effectively reduce folding barriers (*20*, *21*), or by partially unfolding misfolded conformations and hence providing another chance to fold natively (*22*–*25*). GroEL-ES is also thought to act as a passive Anfinsen cage that prevents aggregation, and thus promote folding indirectly (*26*–*28*). Directly testing the elementary folding-promotion mechanisms has proven challenging for chaperones in general, as they are distinguished by specific sequences of microscopic movements, forces, and energy changes that are difficult to follow in time. It is nontrivial to monitor unfolded protein chains throughout their encounter with chaperones and folding process and to detect the compressive or stretching forces that may be exerted on the protein substrate. As a result, it has remained fundamentally unclear how folding transitions are accelerated by chaperones including GroEL-ES (*14*, *15*, *29*).
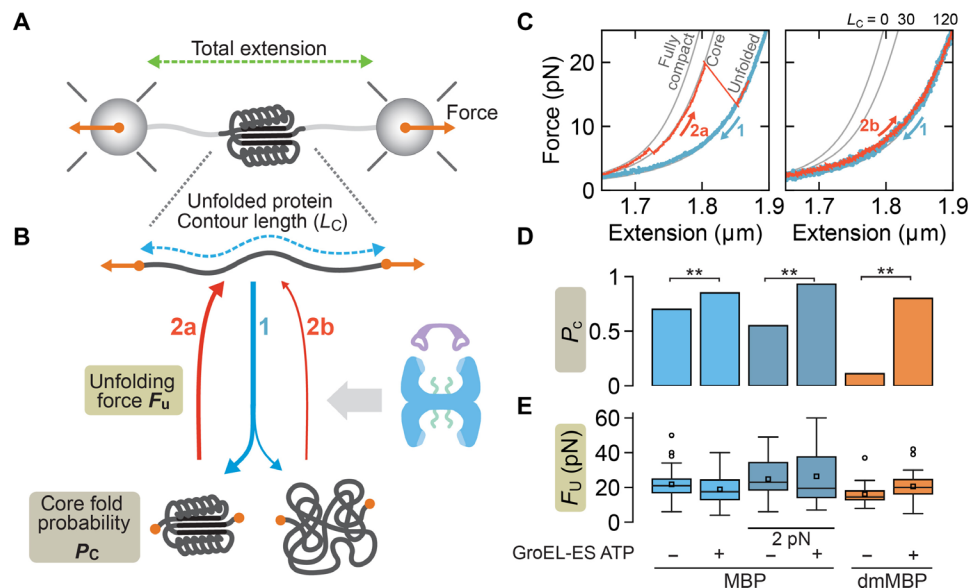
RESULTS

Here, we use optical tweezers and single-molecule fluorescence detection to follow single-substrate proteins in time as they interact with GroEL-ES. We first examined whether GroEL-ES directly stimulated folding of individual maltose-binding proteins (MBPs), which has been used extensively as a GroEL-ES substrate (*21*, *30*), by tethering them to polystyrene beads via DNA handles (*31*, *32*). We exposed unfolded substrates to relax-wait-stretch cycles, by moving the laser beams that trap the beads. After measuring multiple cycles per substrate, for multiple substrates, we quantified the fraction of cycles P_c that show refolding into core MBP states (Fig. 1, A to C). The core MBP fold is the central and major part of MBP that only lacks a number of external α helices, and its formation is rate-limiting in folding (*33*–*35*). The stretching part of the cycle can show unfolding transitions, and hence whether the substrate chain had refolded (Fig. 1C, trace 2A) or had remained unfolded (Fig. 1C, trace 2B). Hence, changes in P_c reflect changes in folding rate rather than folding yield. Note that folding is a probabilistic process, with a cycle that does not show refolding, reflecting an instance where the substrate did not manage to cross the folding barrier, rather than folding yield limitations, and hence can fold in a subsequent cycle. With GroEL-ES and ATP present, we found that P_c increased modestly from 0.7 to 0.85 (Fig. 1D and fig. S1), while the unfolding force F_u remained similar (Fig. 1E). This change in P_c estimates a ratio (R_f) of the folding rates of 1.6, under the simplifying assumption of a single-barrier transition (Materials and Methods). No significant change in the folding of the external α helices onto the core structure was observed in the presence of GroEL-ES and ATP (fig. S1).

Fig. 1. Following single proteins in time shows folding acceleration mediated by GroEL-ES. (**A**) Cartoon of optical tweezers experiments. (**B**) Relax-wait-stretch cycles to quantify MBP core refolding. Unfolded chains (top) are relaxed, kept at 0 pN for 5 s (bottom), or alternatively at 2 pN for 30 s, and stretched to assess the new state. Numbers (1, 2a, and 2b) relate to traces in (C). (**C**) Corresponding force-extension data. After relaxation of unfolded MBP (both panels, blue traces, 1), and waiting at 0 pN, stretching data follow the theoretical WLC curve of the MBP core states (left, red trace 2a) or the unfolded state (right, red trace 2b). Conditions: Buffer in absence of GroEL-ES. (**D**) Fraction of cycles showing core state refolding (P_c), determined as described in (B) and (C). Conditions: Alternating with and without 200 nM GroEL, 500 nM GroES, 1 mM ATP, for MBP substrate and waiting at 0 pN, for MBP at 2 pN, and for dmMBP at 0 pN. ** indicates significant difference ($P < 0.05$) (see fig. S1 and table S1). (**E**) Force at which the protein fully unfolds (F_U), which is found to be approximately constant for different conditions. For dmMBP alone, F_U of the first stretching curve is displayed because of the low refolding rate. Conditions as in (D).

To improve our ability to detect acceleration, the spontaneous folding rate (in the absence of GroEL-ES) was reduced in two ways: (i) Rather than relaxing the chains fully to 0 pN, we maintained a low force (about 2 pN) during the waiting time in the relax-wait-stretch cycles. As a result, the stretched protein chain must now overcome the applied force that counteracts folding, thus limiting the folding rate. (ii) We introduced two mutations in MBP (dmMBP) that may decrease the folding rate (21), while noting another study indicated that they may not (36). We found that P_c decreased to 0.55 and 0.11 (from 0.7) in these two respective experiments (Fig. 1D). Addition of GroEL-ES and ATP now yielded a larger increase in P_c to 0.93 and 0.8, respectively ($R_f = 3$ and 14, respectively; Fig. 1D and fig. S1). Overall, these findings showed folding acceleration of single substrates. The stimulation mechanism remained unresolved, however.

Stabilization of substrate chains in their unfolded state

Because of the complex dynamics of the ATP-driven GroEL-ES cycle (14, 15, 19), we decided to first examine GroEL in different nucleotide-bound states, in the absence of GroES and ATP hydrolysis. Under these conditions, we now detected a behavior of the MBP chains that was not observed in the previous experiments. At a certain moment during the relax-wait-stretch cycling, we sometimes observed a switch from the regular refolding-unfolding behavior to a prolonged unfolded state persisting over multiple relax-wait-stretch cycles, until the tether broke (fig. S2). This switching to a stabilized unfolded state occurred most frequently for GroEL without nucleotides (APO) and GroEL with ATP (50 and 70% of the tethers, respectively). Note that GroEL in the presence of ATP undergoes hydrolysis cycles and hence can be in different nucleotide states

when it interacts with the substrate. Next, we studied the ATP-bound state using the mutant GroEL398A (37) that hydrolyzes ATP slowly (referred to as the ATP* state), and the adenosine 5′-diphosphate (ADP) state by adding not ATP but ADP in solution. We found that switching to a stabilized unfolded state was less frequent in the ATP* and ADP states (30 and 20% of the tethers, respectively). In general, the stabilization of unfolded states is consistent with the known stable binding of unfolded substrates to the apical domains at the rim of the GroEL cavity (38).

Induced collapse of substrate chains

The above experiments presented other notable features. To discuss these, we first note that an idealized noninteracting protein chain coils up like a string when a pulling force is relaxed (Fig. 2A, top cartoons). The protein contour length (L_c) (Fig. 2B) then remains constant, with the worm-like chain (WLC) model describing the decreasing molecular extension (end-to-end distance) and tension (force) (Fig. 2, C and D, left gray curve, see Materials and Methods). However, the measured extension deviated from this WLC behavior and became progressively much smaller, indicating a compaction of the polypeptide chain, down to dimensions of a fully folded protein (Fig. 2D and fig. S3, A to E, blue curves). One can quantify the contour length of the noncompacted part of the chain (L_c) for each measured point using the WLC model, which indeed decreased during the relaxation process (Fig. 2, A to D; and figs. S4, B and C, and S5A). Note that the stochastic motion of the protein chain, the random moments of GroEL binding, and the conformational ensemble of the complexes they may form are causes of variability. Overall, the distance between the C and N termini of the protein chain thus decreases for two reasons: the string-like coiling in
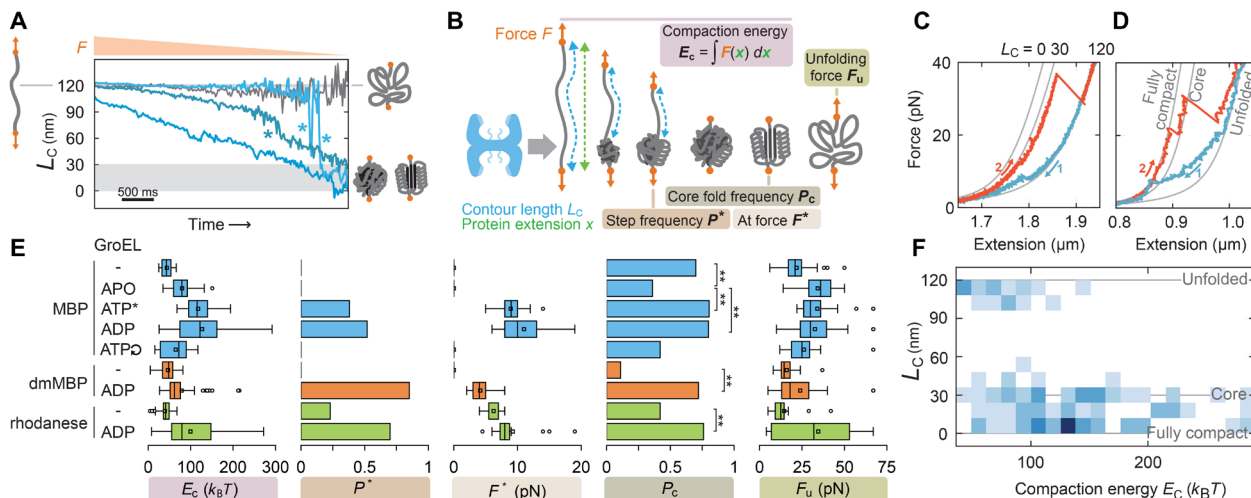
Fig. 2. GroEL can drive protein chain collapse and folding. (A) Contour length (L_c) of unfolded part of dmMBP during force relaxation in presence of GroEL and ADP, showing gradual compaction (blue traces). Stars: Steps indicating (partial) folding. Gray curve represents data without GroEL showing no detectable compaction. Gray bar represents compaction to core state or smaller. **(B)** Cartoon of relax-wait-stretch cycle and measured quantities (see Materials and Methods). P^* indicates the frequency of folding steps during relaxation [see stars in (A)]; F^*, force at which the step occurs; P_c, fraction of cycles showing refolding to the core state (see Fig. 1 and fig. S1); E_c, compaction energy (see fig. S4); and F_u, force required to fully unfold a protein. **(C and D)** Force-extension of relax-wait-stretch cycles, with GroEL and ADP. Relaxation (blue) shows gradual compaction despite counteracting applied force. Numbers indicate temporal order. **(E)** Folding parameters from relax-wait-stretch cycles [see (B)]. Substrates and conditions are as indicated. ATP*, slowly hydrolyzing GroEL398 with ATP; ATP and circular arrow, wild-type GroEL with ATP. ** indicates significant difference ($P < 0.05$). **(F)** L_c of MBP, measured after waiting period at 0 pN, against E_c of the previous relaxation, showing decreasing unfolded states at higher E_c. GroEL-ADP and GroEL398-ATP data were combined.

response to the decreasing applied force and a gradual compaction process in which the compacted part of the polypeptide chain grows in size (Fig. 2B).

To quantify the compaction, we determined the area under the relaxation curves that reflects mechanical work, and we refer to this as the compaction energy E_c (Fig. 2, B and C, and fig. S4). E_c was not zero but comparatively low for MBP alone but was higher with GroEL, specifically in the ATP* and ADP states (Fig. 2, B to E; and fig. S3, B, D, and E). These nucleotide states displayed the weakest apical-domain binding and showed the lowest stabilization of the unfolded conformation (see previous section), strongly suggesting that observed compaction cannot be explained by apical domain binding.

Notably, the gradual compaction was often accompanied by sudden stepwise compaction events (Fig. 2A, stars). These steps suggested folding transitions rather than stable binding: They were large in size (up to nearly the total chain length, Fig. 2A and fig. S3B), occurred at high forces (up to 19 pN; Fig. 2, C to E), and exhibited reversible "hopping" transitions characteristic of folding (Fig. 2A and fig. S3C) (39–41). Moreover, after relaxation and waiting, the polypeptides were often observed in the folded MBP core state, as indicated by subsequent stretching data following the core WLC curve (Fig. 2, C to F) and seen before for spontaneous and GroEL-ES–assisted folding. Notably, the fraction of cycles showing refolded cores was high for the ATP* and ADP states ($P_c = 0.8$; Fig. 2E). P_c increased further beyond 0.95 when the preceding relaxation showed strong compaction ($E_c > 100\ k_BT$; Fig. 2F and fig. S5). Stronger compaction during relaxation of unfolded MBP thus yielded higher core folding probabilities. Overall, these findings showed that compaction was distinct from the stabilization of unfolded states and played rather a role in stimulating folding.

GroEL thus displayed two interaction modes. In the first, unfolded substrates were bound, immobilized, and stabilized. In the second, they were compacted by attractive forces while preserving the necessary mobility to fold. Note that the compaction occurred at substantial forces, well above 10 pN (Fig. 2, D and E, and fig. S3, D and E). Such a collapse process, in which chains compact and form some secondary and tertiary structure is considered key in spontaneous, nonassisted folding and has previously been observed for isolated protein chains using similar force-spectroscopy approaches (33, 42, 43). Two other substrates, dmMBP and rhodanese, displayed similar GroEL-induced collapse enhancement (Fig. 2E and fig. S6). Notably, the slow-folding dmMBP showed a large increase in P_c from 0.11, to more than 0.72 ($R_f = 11$).

Role of the GroEL apical domains

Release of substrate proteins from the GroEL apical domains is relevant to a key window in the GroEL functional cycle, which begins as ATP begins to fill the ring and weaken substrate binding, before GroES binding and encapsulation (14, 15). What happens with the conformation of the substrate in this brief but critical period, and what drives it completely and efficiently into the cavity, is incompletely understood yet could be related to the observed collapse (Fig. 2). Hence, we aimed to detune the affinity of the apical domains for unfolded substrate proteins. Saturating the GroEL ring with ADP is an ideal condition for this purpose, as its stability in time (no ATP turnover) is crucial to our real-time analysis, and our results discussed above showed that binding was comparatively weak (substrate stabilization in the unfolded state was at a low 20%). To further reduce the affinity, we added small peptides equivalent to the unstructured GroES loops (Fig. 3A), which compete for the apical domain substrate binding sites (44). In relax-wait-stretch
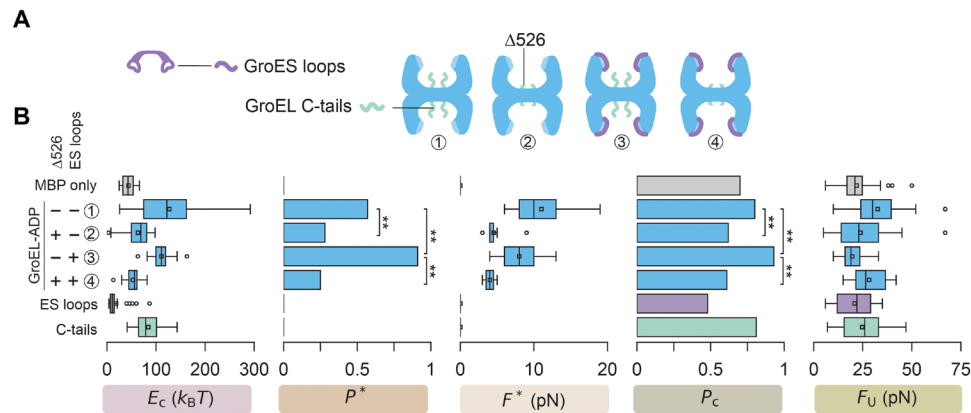
Fig. 3. Roles of the GroEL apical domains and cavity. (**A**) Measured GroEL variants. To tune down the GroEL apical domain affinity for unfolded substrates, unstructured loops of GroES are added as separate polypeptides (purple) that bind the GroEL apical domains using the GroEL state that shows the weakest ability to stabilize unfolded states (the ADP state). The effect of the unstructured C-terminal tails (light green) of GroEL is tested by truncation (GroELΔ526). (**B**) Parameter quantification from relax-wait-stretch cycles in different conditions (see Fig. 2B): Total compaction energy during relaxation (E_c), fraction of relaxation curves with steps (P^*) at force (F^*), core refold probability after 5 s at 0 pN (P_c), unfolding force or maximally sustained force (F_U), as determined from MBP relax-stretch cycles. Conditions, top to bottom: No chaperone, GroEL, GroELΔ526, GroEL and GroES loops, GroELΔ526 and GroES loops, GroES loops only, and C-tails only. See table S1. ** indicates significant difference ($P < 0.05$).

experiments on MBP, the sudden stabilization of unfolded chains (fig. S2) was indeed no longer observed under these conditions, consistent with reduced apical domain affinity. Notably, we also found that the fraction of cycles with folding steps during relaxation (P^*), as well as P_c, still showed an increase relative to MBP alone (Fig. 3, A and B). For dmMBP, which exhibited lower spontaneous folding probabilities (Fig. 2E), these increases were more prominent (fig. S7). They were not caused by the GroES loops directly, as they alone did not yield increases (Fig. 3B). These data indicated that reducing the apical domain affinity reduced the ability to stabilize unfolded states while maintaining the capacity to promote folding transitions, consistent with the apical domains antagonizing folding.

The apical domains also exhibited another effect: The observed unfolding force F_u of MBP, which had increased with GroEL, now decreased back to MBP-only levels when the GroES loops were present (Figs. 2E and 3 and fig. S8). dmMBP showed a similar trend (fig. S7). These data indicated that GroEL can stabilize refolded states against forced unfolding, in addition to stabilizing unfolded states, while binding of the GroES loops suppressed both effects. These contrasting GroEL effects should depend on the binding dynamics. Upon their encounter, if the unfolded chain binds the apical domains sufficiently strongly, this unfolded state can be stabilized. When the chain is released or fails to bind stably, pathways open up to partially folded states. Surfaces of the latter may expose regions that are covered in the fully folded state and hence be stabilized through interactions with GroEL. The finding that compaction and folding remained stimulated in the presence of GroES loops (Fig. 3B) also suggested that parts of GroEL other than the apical domain–binding sites were relevant.

Role of the GroEL C-terminal tails
To test whether the GroEL interior played a role in the folding stimulation, we truncated the unstructured C-terminal tails at the cavity bottom (GroELΔ526) (45). P_c and P^* were indeed more than twofold lower for GroELΔ526 than for GroEL, both with and without the GroES loops present (Fig. 3, A and B, and fig. S7, ADP present). Even alone, the C-tails could promote some compaction (Fig. 3B). However, P_c and P^* did not change significantly, indicating that

they were not sufficient to promote folding. Overall, the data showed that GroEL-mediated collapse and folding depended on the C-tails in the GroEL cavity. The enhancement of chain collapse while maintaining the dynamics that is required for folding upon interaction with GroEL is notable and suggests a balance between different cavity properties (11, 21, 45).

The substrate-chaperone complex
Last, we sought to verify two key interactions of the substrate-chaperone complex in these experiments, which required different approaches. To directly visualize GroEL-substrate binding, we scanned a fluorescence excitation beam along the tethered MBP during relax-wait-stretch cycles at constant velocity (Fig. 4A). Atto532-labeled GroEL was present at reduced concentrations to limit background fluorescence, as well as ADP. The appearance of a fluorescent spot between the beads indicated binding of a single GroEL tetradecamer (Fig. 4B, yellow triangle). Folding events were simultaneously reported by the tweezers measurements (Fig. 4C, green triangle), in a similar manner as shown previously (Fig. 2B). Consistently, during relaxation, such GroEL-binding events always occurred first, and folding steps afterward (Fig. 4D). These findings confirmed stimulated folding transitions in substrates complexed with GroEL.

Second, we used a buffer-exchange protocol to verify that ternary complexes (GroEL-GroES-MBP) can indeed be formed in the optical tweezers assay. We used the single-ring GroEL variant (SR1) for this purpose (46). GroES binding to SR1 is known to trap the latter in the ADP-bound state with ATP present, and hence irreversibly lock GroES-SR1 together (14, 15). The binding of GroES to the SR1 apical domains is also believed to displace substrates from the apical domains into the SR1-GroES cavity.

First, we complexed SR1 to unfolded MBP. Hence, we unfolded MBP in the presence of SR1 and ATP. Subsequent inability of MBP to refold during multiple relax-wait-stretch cycles indicated that SR1 had bound to the unfolded MBP chain (Fig. 4, E and F). The beads and tethered MBP were then moved to another channel in the microfluidic device, which contained a medium with GroES and ATP only. Here, SR1 was not present in solution to prevent premature
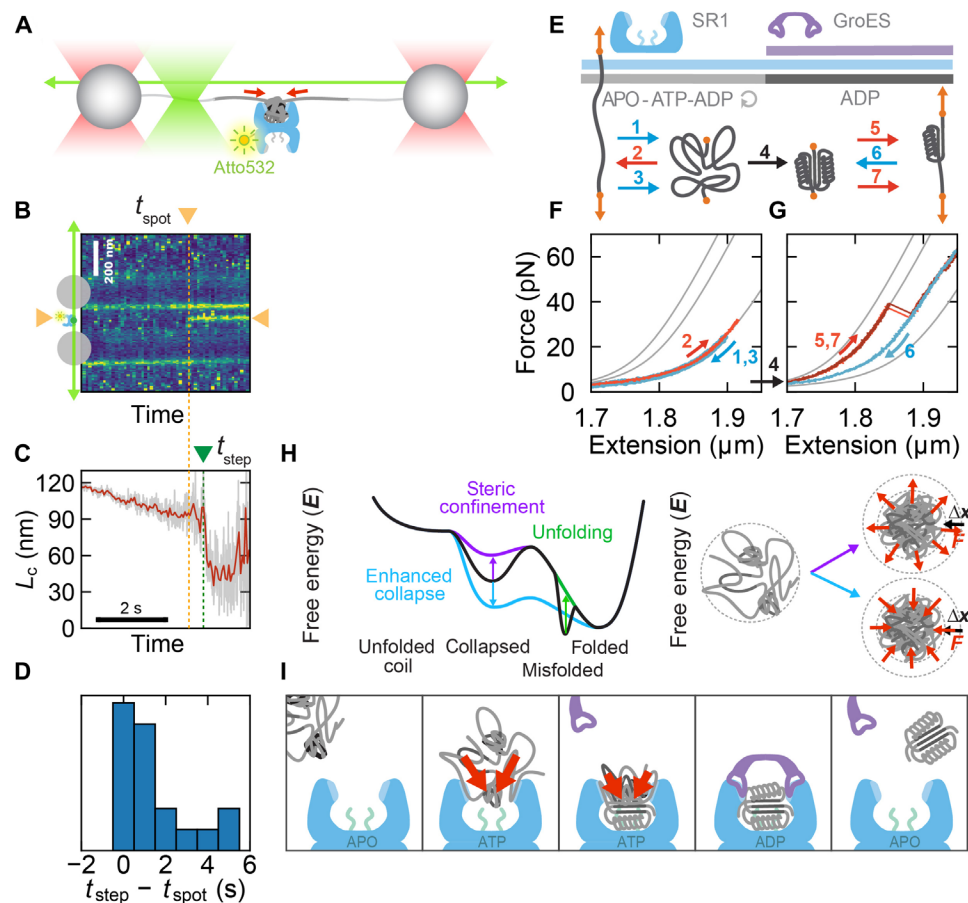
Fig. 4. Compaction and folding in a single GroEL tetradecamer. (**A**) Setup to detect substrate-GroEL complex during stimulated folding (B to D): optical tweezers (red), scanning fluorescence excitation (green), Atto532-labeled GroEL (blue, ~15 nM), and ADP. (**B**) Corresponding fluorescence emission kymograph during force relaxation. Fluorescent spot appearing at t_{spot} shows single GroEL binding. Continuous horizontal bright lines represent bead fluorescence. (**C**) Corresponding contour length shows folding step at t_{step}. (**D**) Time difference shows that folding occurs after GroEL binding. (**E**) Buffer exchange protocol and MBP folding events during SR1-GroES-MBP complex formation (F and G). (**F**) MBP remains unfolded during relaxation-stretching cycles (1 to 3), in the presence of SR1 and ATP, indicating SR1 is bound. (**G**) After buffer exchange to GroES with ATP (4), stretching (5) shows MBP is now folded, and unfolds partially, and after relaxation (6), it is folded again (7). (**H**) Energy landscape cartoons for folding stimulation models. Green: GroEL exerts unfolding forces on misfolded states. Purple: Steric confinement increases free energy. Blue: enhanced collapse lowers free energy and barrier. (**I**) Cartoons of event sequence suggested by our data. Red arrows indicate compaction forces induced by GroEL.

binding and depletion of GroES. In this manner, the substrate and substrate bound SR1 were moved to the new channel, while unbound SR1 in solution was washed away. This exposure to GroES and ATP was found to trigger MBP refolding to the core state, which in subsequent stretching did not unfold fully (Fig. 4G and fig. S10).

These data strongly suggested a SR1-ES-MBP complex. If GroES had failed to bind and only SR1 was bound, MBP would have remained unfolded (Fig. 4F). Moreover, the observed refolding upon exposure to GroES is consistent with the known role of GroES in competing substrates off the SR1 apical domains and displacing them into the SR1 cavity, where they subsequently fold. Last, after SR1 and GroES exposure, refolded MBP substrates could not be unfolded fully even at 60 pN (Fig. 4G and fig. S10). This behavior and stability are notable and indeed are not observed for the other conditions. These data gave further evidence that SR1 had not unbound MBP and rather indicated that the refolded MBP was in complex with SR1 and GroES, which stabilized it against forced unfolding. Steric constraints may play a role here, as bound GroES could prevent encapsulated structures to move out of the cavity, and

hence increase the unfolding force. GroES may not be symmetrically sealed and bound to all seven SR1 monomers, as seen in structural work (*47*), and indeed such intimate contacts may not be required to initiate folding. It was shown that polypeptides can be sandwiched in between GroEL and GroES and hence protrude partly outside the cavity (*48*). In our substrates, the core MBP structure is flanked by flexible N- and C-terminal segments that could similarly provide such a connection to the outside (see Materials and Methods), thus allowing the MBP core to be encapsulated in the SR1-GroES cavity.

DISCUSSION
The GroEL-ES–stimulated folding mechanism we present, in which enhanced collapse plays a central role, is distinct from current models (Fig. 4, H and I) (*14, 15, 21, 49*). In confinement models, steric repulsion forces exerted by the walls of the GroEL-ES cavity are proposed to decrease the chain entropy of the nonnative substrate protein and thus increase its free energy, which effectively lowers folding barriers. In unfolding models, pulling forces that are applied

to misfolded states also increase chain free energy and are proposed to allow escape to productive folding trajectories. Here, we measured GroEL-induced forces and found that they are contractile and enhance protein chain collapse. Such compaction suggests a decreased chain free energy rather than an increased one (Fig. 4H). The observed increases in folding probabilities specifically imply that the folding barrier height was reduced (Fig. 4H). Indeed, the nonassisted collapse of unfolded protein chains is known to lower kinetic folding barriers by bringing residues together that must make contact in the folded structure (8, 9, 43). Note that these models are not mutually exclusive and could even facilitate each other. For instance, the forces that drive the collapsing chain into the cavity may help unfold kinetically trapped misfolded substrates that are partly bound to the apical domains (Fig. 4I).

The presented single-molecule analysis sketches the following picture for the conformational trajectories of unfolded substrates as they interact with GroEL. At the start of the GroEL-ES functional cycle (Fig. 4I), substrates are stabilized in their unfolded state by binding the GroEL apical domains (fig. S2) and can also interact with the C-terminal tails (25, 45, 50). Folding completion ultimately depends on full release of the substrate protein following GroES binding, while GroEL also converts from the ATP to the ADP state (15). Yet, mobilization, partial release, and the initiation of substrate protein collapse can begin before full encapsulation (Figs. 1, 3, and 4, E to G). Chain segments displaced into the cavity can undergo a stimulated gradual compaction and discrete folding steps. Protein chains are known to collapse autonomously (8, 9, 43), compact protein substrates have been observed in GroEL-ES and other chaperones including Spy (11, 51), and a sequential release of substrate segments from the GroEL cavity wall has been proposed to produce a controlled stepwise collapse of substrate chains (49). Here, we directly detected the collapse of unfolded substrates and found that can be strengthened by GroEL and hence stimulate folding transitions.

The stimulation of folding transitions by the GroEL ring is a notable feature of our data. Several studies have reported folding improvements by GroEL, but whether this reflects aggregation inhibition or folding acceleration has remained unclear (14, 15). At the same time, standard ensemble assays have suggested that GroEL-stimulated folding of dmMBP depends on GroES and ATP (21, 27), a result we corroborate here using a tryptophan (Trp) fluorescence assay (fig. S9). These data highlight key assay differences. First, the optical trap assay detects distinct conformational transitions that occur on the time scale of a few seconds. By contrast, the Trp fluorescence signal evolves over tens of minutes and can indeed be affected by various steps that can be slow, such as reversible aggregation and apical domain dissociation, and other conformational transitions that affect the local environment around the Trp residues. Second, the single-molecule data indicated two opposing effects that average out in the bulk assay: GroEL apical domain interactions that delay folding and GroEL cavity interactions that accelerate folding. Third, there are many differences in experimental details, such as substrate concentration, competing aggregation, residual chemical denaturants, and specific substrate conformations. These factors can affect how dominant the above slow steps are and hence whether it is possible to detect folding acceleration. While the dmMBP substrates are tethered in the single-molecule assay, entropic effects are minor, specifically at low force (39–41) where P_c is quantified. They oppose rather than promote folding, and GroEL-ES is observed to stimulate protein folding, nonetheless.

The physical effects that underlie protein collapse enhancement may be similar to notions advanced in theoretical studies on the role of water within the GroEL-ES cavity (52). More generally, charged and hydrophobic surfaces in particular in confined volumes, as well as amphiphilic solutes, can modulate the hydrophobic effect (53), which in turn is the driving force in protein chain collapse. The control of collapse and folding by interacting proteins, as observed here, provides the possibility of local modulation and allosteric regulation of these effects.

GroEL-ES is known to support a broad range of proteins, and collapse is pervasive in unfolded proteins. One may speculate that nonoptimal polypeptide collapse is a more general folding impediment that GroEL-ES helps resolve. Collapse enhancement by GroEL-ES can thus limit the lifetime of aggregation-prone collapsed states and could help transferring substrates from Hsp70 to GroEL, as Hsp70-bound substrates may be pulled into the GroEL cavity that Hsp70 cannot enter. Moreover, we found that collapse modulation does not require the closed cavity that is unique to GroEL-ES. The ability to manipulate collapsed protein states may thus be exploited more generally within the protein quality control machinery to regulate folding and intrinsic disorder.

MATERIALS AND METHODS

Expression and purification of MBP, dmMBP, and rhodanese
MBP and dmMBP were overexpressed in T7 competent cells [New England Biolabs (NEB) laboratories] in LB medium supplemented with 0.2% glucose and kanamycin (50 µg/ml) at 30°C until OD_{600} (optical density at 600 nm) ~0.6, induced with 0.4 µM isopropyl-β-D-thiogalactopyranoside (IPTG) (Sigma-Aldrich), and incubated at 18°C overnight. The culture was harvested by centrifugation at 5000g for 20 min at 4°C. All following steps were carried out at 4°C. The pellet was resuspended in ice-cold buffer A [50 mM phosphate buffer (pH 7.5), 200 mM NaCl, 10 mM EDTA, 50 mM glutamic acid–arginine (Sigma-Aldrich), and 3 mM β-mercaptoethanol (Sigma-Aldrich)] and lysed using an Emulsiflex homogenizer. The lysate was cleared from cell debris by centrifugation at 50,000g for 1 hour, followed by incubation with Amylose resin (NEB) for 1 hour. After extensive washing with buffer A, the proteins were eluted using buffer A supplemented with 20 mM maltose.

For rhodanese, the pellet was resuspended in buffer B [100 mM tris-HCl (pH 7.0), 5 mM EDTA, 20 mM $Na_2S_2O_3$, and 2 mM β-mercaptoethanol] and lysed as described above. The lysate was mixed with Protino Ni-NTA Agarose (Macherey-Nagel) and incubated for 1 hour. After washing, the protein was eluted with buffer B supplemented with 250 mM imidazole.

Purification of GroEL, GroES, and their variants
GroEL was expressed from an inducible plasmid in *Escherichia coli* BL21 in LB at 37°C (51). After cell disruption, the crude lysate was clarified by ultracentrifugation (142,000 relative centrifugal force), followed by anion exchange chromatography (FastFlow Q, GE) equilibrated in buffer C [50 mM tris (pH 7.4), 0.5 mM EDTA, and 2 mM dithiothreitol (DTT)] and eluted by linear gradient from 7.5 to 35% with buffer D [50 mM tris (pH 7.4), 0.5 mM EDTA, 2 M NaCl, and 2 mM DTT]. GroEL fractions were concentrated by 70% (w/v) ammonium sulfate precipitation. This precipitate was solubilized and dialyzed against 50 mM bis-tris (pH 6.0), 50 mM KCl, 0.5 mM EDTA, 2 mM DTT containing 25% (wild-type GroEL) or 12.5%

(all GroEL mutants) methanol. A second round of strong anion exchange (FastFlow Q, GE), run in the same methanol-containing buffer at pH 6.0, was used to strip copurifying small proteins and peptides from the GroEL oligomers. To further remove contaminating proteins and peptides that remain tightly associated through prior stages of purification, GroEL fractions were gently agitated in the same methanol-containing buffer and Affi Blue Gel (Bio-Rad) resin overnight at 4°C under an argon atmosphere. The final sample was dialyzed into storage buffer [25 mM tris (pH 7.4), 100 mM KCl, 0.5 mM EDTA, and 2 mM DTT], supplemented with glycerol [15 to 20% (v/v)], concentrated, and snap frozen using liquid nitrogen.

GroES was expressed from an inducible plasmid in *E. coli* BL21(DE3) in LB at 37°C. After cell disruption, the crude lysate was clarified by ultracentrifugation (142,000 rcf), followed by acidification with sodium acetate, and cation exchange chromatography (FastFlow S, GE) equilibrated in buffer E [50 mM NaOAc (pH 4.6), 0.5 mM EDTA, and 2 mM DTT] and eluted by linear gradient from 0 to 25% buffer F [50 mM NaOAc (pH 4.6), 0.5 mM EDTA, 2 M NaCl, and 2 mM DTT]. The sample was dialyzed against 25 mM tris (pH 7.4), 0.5 mM EDTA, 50 mM KCl, and 2 mM DTT and applied to a strong anion exchange column (Source Q, GE). GroES was eluted with NaCl, and enriched fractions were pooled. The sample was dialyzed into storage buffer supplemented with glycerol [15 to 20% (v/v)], concentrated, and snap frozen using liquid nitrogen.

For the expression of SR1, *E. coli* BL21 DE3 transformed with pSR1 was grown in LB-ampicillin (100 μg/ml) at 30°C to an OD$_{600}$ of 0.5. Overexpression was induced by adding 1 mM IPTG, and growth was continued for 3 hours. Cells were harvested by centrifugation and stored at −70°C after flash freezing in liquid nitrogen. Frozen cells were resuspended in 20 mM tris-HCl (pH 7.4), 50 mM KCl, 1 mM EDTA, 1 mM DTT, and 1 mM phenylmethylsulfonyl fluoride, lysed using a French press, and cell debris were removed by centrifugation. SR1 was enriched by fractionated $(NH_4)_2SO_4$ precipitation between 35 and 45% saturation. Following dialysis in 50 mM tris-HCl (pH 8), 1 mM EDTA at 4°C, the protein solution was fractionated using a DEAE Sepharose Fast Flow anion exchange chromatography resin (GE Healthcare) eluting with a gradient from 0 to 1 M NaCl and further fractionated by size exclusion chromatography using a HiPrep 26/60 Sephacryl S-500 HR column. SR1-containing fractions were pooled, concentrated using Amicon Ultra centrifugal filters (Merck), frozen in liquid nitrogen, and stored at −70°C.

GroEL labeling
The GroEL variant (EL315C) (*54*) was labeled with Atto-532 maleimide (Sigma-Aldrich). Reactive dyes were prepared fresh from dry powder in anhydrous dimethylformamide (DMF) immediately before use. All proteins were first buffer exchanged 300× to 400× the original volume by a Vivaspin Turbo 15 (Satorious) into 50 mM tris buffer (pH 7.4), 100 mM KCl, 0.5 mM EDTA, and 1 mM TCEP. The proteins were then run over gel filtration (PD-10 column, Pharmacia) equilibrated in reaction buffer [50 mM tris (pH 7.4), 100 mM KCl, 0.5 mM EDTA, and 0.5 mM TCEP]. EL315C was concentrated to a final concentration of 70 μM (monomer) in a volume of 5 ml. Protein samples were added to individual 5-ml conical Weaton reaction vials, followed by two sequential reactive dye additions. Freshly prepared Atto-532 maleimide in DMF was added at a molar ratio of 1:6.5 to EL315C monomer. Following each addition, the sample was incubated for 45 min in the dark at 23°C. Following

the full 1.5-hour reaction time, the sample was quenched by addition of 5 mM glutathione. The labeled EL315-Atto532 was separated from unreacted dye by four rounds of dilution and concentration in a Vivaspin Turbo 15 (Sartorious), followed by gel filtration (PD-10 column, Pharmacia). The labeled proteins were then supplemented with glycerol (15 to 20%) and snap frozen using liquid nitrogen. Protein concentration was determined using a calibrated Bradford assay in which the protein standard was from a sample of wild-type GroEL whose concentration had been previously established. Conjugated dye concentrations are determined by absorption spectroscopy of the denatured proteins (in 6 M Gdm buffer) using the following corrected extinction coefficient: Atto-532, 115,000 M^{-1} cm^{-1}. GroEL-Atto 532 activity was confirmed by methylthioguanosine (MESG) adenosine triphosphatase activity assay (EnzChek, Molecular Probes) and native gel filtration (Superdex 200, GE).

GroES mobile loops and GroEL C-tails
The GroES mobile loops (*44*) ETKSAGGIVLTGS and GroEL C-tails (GGM)$_4$M were ordered from GenScript. GroES mobile loops and C-tails were dissolved in Milli-Q water and snap frozen using liquid nitrogen. Before measurements, the samples were dissolved in HMK buffer [50 mM Hepes (pH 7.5), 5 mM MgCl$_2$, and 100 mM KCl]. The GroES mobile loops were added in fivefold molar excess (*44*) to GroEL during optical tweezers experiments (Fig. 3, A and B, and fig. S7).

Protein-DNA constructs
The cysteines at the N and C termini of proteins were coupled with 20–base pair (bp) maleimide single-stranded DNA oligos at 37°C for 1 hour. DNA tethers (2.5 and 1.3 kbp) were generated by polymerase chain reaction (PCR) from pUC19 plasmid (NEB) with a double digoxigenin– or biotin-labeled primer on one side and a phosphoprimer on the other side. Purification was done with a QIAquick PCR purification kit (Qiagen). The phosphorylated strand was digested by lambda exonuclease (NEB) for 2 hours at 37°C and purified using an Amicon 30-kDa molecular weight cutoff (MWCO) filter (Merck). Deep Vent (exo-)DNA polymerase (NEB) and a 20–nucleotide (nt) more upstream primer than the phosphoprimer from the PCR were used for the fill-up of the second DNA strand, creating a 20-nt overhang. This overhang is complementary to the 20-nt oligonucleotide sequence coupled to the termini of proteins. The overhang DNA was added to the protein-oligo chimera together with T4 ligase (NEB) and incubated for 30 min at 16°C, followed by 30 min on ice. The resulting protein-DNA hybrid was flash frozen and stored at −80°C until measurement.

Optical tweezers experiments
NeutrAvidin-coated beads (2.1 μm) were purchased from Spherotech and stored at 4°C until use. Anti-digoxigenin beads were prepared by coating carboxylated polystyrene beads (2.1 μm, Spherotech) with anti-digoxigenin antibodies from Sigma-Aldrich using a carbodiimide reaction (PolyLink Protein Coupling Kit, Polysciences Inc.) The protein-coated beads were prepared by mixing 50 ng of MBP, dmMBP, or rhodanese constructs with anti-digoxigenin beads in 10 μl of HMK buffer. The mixture was then incubated at 4°C for 30 min on a rotary mixer. Next, the beads were dissolved in 400 μl of HMK buffer for optical tweezers experiments. Optical tweezers measurements were done in HMK buffer. ADP and ATP solutions were prepared by dissolving ADP and ATP sodium salt from Sigma-Aldrich

in HMK buffer. Experiments in GroEL ADP conditions were verified using ultrapure ADP (99.9%; Gentaur).

Stretch-relax experiments were performed on two optical tweezers setups. The first was a custom-built single-trap instrument. A substrate-coated anti-digoxigenin bead was held in the optical trap, and a NeutrAvidin bead was placed on the end of a micropipette tip. The two beads were brought in close contact, allowing a tether between the beads to form. Proteins were stretched and relaxed by moving the flow cell and micropipette with a nanopositioning piezo stage at 50-nm/s speed, which corresponds to a pulling rate of 5 pN/s. The deflection of the bead in the trap was measured using quadrant photodiode at 50 Hz. The data were filtered with a fifth-order Butterworth filter at 20 Hz. The optical traps were calibrated by recording the power spectrum of the Brownian motion of the beads (55) yielding stiffnesses ranging from 120 to 170 pN/μm.

The second setup was a dual-trap optical tweezers instrument (C-trap from Lumicks). As described above, tethers were formed by bringing similarly prepared construct-coated and NeutrAvidin beads in close proximity. The protein was stretched and relaxed at a constant velocity of 50 nm/s, by moving one of the traps. The data were acquired at 500 kHz and averaged to 500 Hz. For constant force measurements, tension was held at 2 pN on average for 30 s using a proportional-integral-derivative feedback loop, before pulling again at constant velocity (Fig. 1E). In fig. S3C, the distance between the traps is constant, while the extension of the protein is monitored as it changes conformation. Note that the beads can change position within the traps. For fluorescence measurements in combination with constant velocity stretch-relax experiments (Fig. 4, A to D), Atto-532–labeled GroEL proteins were visualized using a green excitation laser (532 nm), with 2 mM Trolox and 4 mM β-mercaptoethanol in the buffer. The labeled GroEL proteins were injected at 100 nM concentration; however, because of concentration gradients in the flow cell, the measurements were performed in channels with lower concentrations (<15 nM) to reduce the background signal. The excitation beam was used to scan along the tethered construct at 10 Hz during the force-spectroscopy measurements, generating fluorescence kymographs that were aligned to the force signal using ImageJ and custom-built Python code.

Trp fluorescence experiments

For spontaneous dmMBP folding (fig. S9), 980 μl of folding buffer (50 mM Hepes, 200 mM KCl, 10 mM MgoAc, and 2 mM DTT) was added to a 1-ml thermally jacketed cuvette and equilibrated to 23°C in a T-format fluorometer for 2 min with stirring. Then, 20 μl of dmMBP was rapidly injected (~2 s of dead time) into the cuvette, yielding a final dmMBP concentration of 100 nM. Trp fluorescence was monitored continuously from the point of injection to 10 min. To form a GroEL-dmMBP binary complex, GroEL was first diluted into folding buffer to a final concentration of 200 nM at room temperature in a 1-ml Eppendorf tube. Twenty microliters of dmMBP was pipetted onto the inside of the cap of the Epperdorf tube for a final concentration of 100 nM. Simultaneously, the lid was closed, and the solution was repeatedly mixed by inversion for 5 s, followed by incubation of the sample for 5 min at room temperature. For dmMBP refolding in the presence of GroES, 400 nM GroES was added to a sample of the GroEL-dmMBP binary complex and incubated for 1 min at room temperature. Solutions were pipetted into the fluorometer cuvette and equilibrated at 23°C for 2 min with stirring. Addition of ATP or ADP was carried out by rapid injection

(final concentration of 2 mM) into the cuvette, and Trp fluorescence was monitored continuously from the point of injection to 10 min. In all cases, fluorescence measurements were carried out using 295 ± 2 nm excitation, and emission was collected 345 ± 2 nm.

Data analysis

Several checks were performed to confirm that the data corresponded to a proper single tether, which include comparing the total measured unfolded length to the expected length, consistency with the WLC model (56) (at higher forces), overstretching at 67 pN, and final tether breakage in one clean step. The unfolding forces (F_U), contour lengths (L_C), refolding forces (F^*), and compaction energies (E_C) were quantified from force extension data (constant velocity) using an open-source MATLAB code (57) after modifications. F_U was determined from stretching traces as the force required to fully unfold a protein [Figs. 1 (C, left, and E), 2 (C to E), and 3, and fig.S7]. For stretching traces in which the protein did not fully unfold below the maximum force that could be applied (67 pN, corresponding to the DNA overstretching plateau), F_U was determined as 67 pN, the maximally sustained force (Fig. 2E and fig. S8). The contour lengths (L_c) of refolded states were determined from the force-extension data of the stretching curve before the first unfolding transition, using the WLC model (fig. S1, A and B). The persistence lengths of the DNA (45 nm) and protein (1.5 nm) and the stretch modulus of DNA (1200 pN) were the fixed parameters in the WLC model. The MBP substrate consists of a core structure flanked at the N terminus by a nine-residue segment, consisting of five native residues and an engineered four-residue flexible linker that in turn connects to the DNA strand, and at the C terminus by a longer segment of 88 residues, which also connects to a DNA strand. In Figs. 2A and 4C, the instantaneous protein contour length was calculated using the same WLC model. Compaction energy (E_C) was calculated by quantifying the area under the relaxation curve and then subtracting the area under the WLC curve for fully unfolded protein [Figs. 2E and 4 (B and C) and fig. S7]. P^* was determined as the fraction of relaxation traces that show (one or more) steps in L_c of more than 15 nm (Figs. 2E and 3 and fig. S7). F^* was quantified as the measured force just before such a step in L_c (during relaxation, Figs. 2E and 3 and fig. S7). The folding probability (P_c) was quantified as the fraction of relax-stretch cycles showing refolding to the core MBP state (Figs. 2E and 3 and figs. S1 and S7). R_f is the ratio of the refolding rates for two (chaperone) conditions, under the simplified assumption of a single-barrier folding process and is estimated as $\frac{\ln(1 - P_{c2})}{\ln(1 - P_{c1})}$ where P_{c1} and P_{c2} are the folding probabilities of the two conditions (33). In Fig. 4 (B to D), the t_{step} and t_{spot} values were measured using ImageJ and custom-built Python code.

Statistical analysis

The statistical significance of differences in folding probability (P_c) and refolding at force probability (P^*) between experimental conditions was calculated using one-tailed two proportion z test. The statistical significance of differences in compaction energy (E_c) and maximally sustained forces (F_U) between experimental conditions was calculated using two-sample assuming unequal variance t test. Test results are mentioned as P values in the main text. In box charts, whiskers indicate 90 and 10% extreme values, the inner line represents the median, the length of the box indicates interquartile range, and the inner small square is the mean of the population.

SUPPLEMENTARY MATERIALS

Supplementary material for this article is available at https://science.org/doi/10.1126/sciadv.abl6293

View/request a protocol for this paper from *Bio-protocol*.

REFERENCES AND NOTES

1. D. Thirumalai, H. S. Samanta, H. Maity, G. Reddy, Universal nature of collapsibility in the context of protein folding and evolution. *Trends Biochem. Sci.* **44**, 675–687 (2019).
2. K. A. Dill, D. J. Shortle, Denatured states of proteins. *Annu. Rev. Biochem.* **60**, 795–825 (1991).
3. G. J. Haran, How, when and why proteins collapse: The relation to folding. *Curr. Opin. Struct. Biol.* **22**, 14–20 (2012).
4. L. P. Bergeron-Sandoval, N. Safaee, S. W. Michnick, Mechanisms and consequences of macromolecular phase separation. *Cell* **165**, 1067–1079 (2016).
5. C. M. Dobson, Protein folding and misfolding. *Nature* **426**, 884–890 (2003).
6. J. Habchi, P. Tompa, S. Longhi, V. N. Uversky, Introducing protein intrinsic disorder. *Chem. Rev.* **114**, 6561–6588 (2014).
7. Y. Shin, C. P. Brangwynne, Liquid phase condensation in cell physiology and disease. *Science* **357**, (2017).
8. I. Peran, A. S. Holehouse, I. S. Carrico, R. V. Pappu, O. Bilsel, D. P. Raleigh, Unfolded states under folding conditions accommodate sequence-specific conformational preferences with random coil-like dimensions. *Proc. Natl. Acad. Sci. U.S.A.* **116**, 12301–12310 (2019).
9. A. S. Holehouse, R. V. Pappu, Collapse transitions of proteins and the interplay among backbone, sidechain, and solvent interactions. *Annu. Rev. Biophys.* **47**, 19–39 (2018).
10. J. A. Riback, M. A. Bowman, A. M. Zmyslowski, C. R. Knoverek, J. M. Jumper, J. R. Hinshaw, E. B. Kaye, K. F. Freed, P. L. Clark, T. R. Sosnick, Innovative scattering analysis shows that hydrophobic disordered proteins are expanded in water. *Science* **358**, 238–241 (2017).
11. S. Hiller, Chaperone-bound clients: The importance of being dynamic. *Trends Biochem. Sci.* **44**, 517–527 (2019).
12. M. P. Mayer, Gymnastics of molecular chaperones. *Mol. Cell* **39**, 321–331 (2010).
13. S. Walter, J. Buchner, Molecular chaperones—Cellular machines for protein folding. *Angew. Chem. Int. Ed. Engl.* **41**, 1098–1113 (2002).
14. M. Hayer-Hartl, A. Bracher, F. U. Hartl, The GroEL-GroES chaperonin machine: A nano-cage for protein folding. *Trends Biochem. Sci.* **41**, 62–76 (2016).
15. Z. Lin, H. S. Rye, GroEL-mediated protein folding: Making the impossible, possible. *Crit. Rev. Biochem. Mol. Biol.* **41**, 211–239 (2006).
16. D. K. Clare, D. Vasishtan, S. Stagg, J. Quispe, G. W. Farr, M. Topf, A. L. Horwich, H. R. Saibil, ATP-triggered conformational changes delineate substrate-binding and -folding mechanics of the GroEL chaperonin. *Cell* **149**, 113–123 (2012).
17. M. J. Cliff, C. Limpkin, A. Cameron, S. G. Burston, A. R. Clarke, Elucidation of steps in the capture of a protein substrate for efficient encapsulation by GroE. *J. Biol. Chem.* **281**, 21266–21275 (2006).
18. M. Taniguchi, T. Yoshimi, K. Hongo, T. Mizobata, Y. Kawata, Stopped-flow fluorescence analysis of the conformational changes in the GroEL apical domain: Relationships between movements in the apical domain and the quaternary structure of GroEL. *J. Biol. Chem.* **279**, 16368–16376 (2004).
19. M. Yokokawa, C. Wada, T. Ando, N. Sakai, A. Yagi, S. H. Yoshimura, K. Takeyasu, Fast-scanning atomic force microscopy reveals the ATP/ADP-dependent conformational changes of GroEL. *EMBO J.* **25**, 4567–4576 (2006).
20. A. Brinker, G. Pfeifer, M. J. Kerner, D. J. Naylor, F. U. Hartl, M. Hayer-Hartl, Dual function of protein confinement in chaperonin-assisted protein folding. *Cell* **107**, 223–233 (2001).
21. K. Chakraborty, M. Chatila, J. Sinha, Q. Shi, B. C. Poschner, M. Sikor, G. Jiang, D. C. Lamb, F. U. Hartl, M. Hayer-Hartl, Chaperonin-catalyzed rescue of kinetically trapped states in protein folding. *Cell* **142**, 112–122 (2010).
22. D. Thirumalai, G. H. Lorimer, Chaperonin-mediated protein folding. *Annu. Rev. Biophys. Biomol. Struct.* **30**, 245–269 (2001).
23. H. S. Chan, K. A. Dill, A simple model of chaperonin-mediated protein folding. *Proteins* **24**, 345–351 (1996).
24. Z. Lin, D. Madan, H. S. Rye, GroEL stimulates protein folding through forced unfolding. *Nat. Struct. Mol. Biol.* **15**, 303–311 (2008).
25. J. Weaver, M. Jiang, A. Roth, J. Puchalla, J. Zhang, H. S. Rye, GroEL actively stimulates folding of the endogenous substrate protein PepQ. *Nat. Commun.* **8**, 15934 (2017).
26. R. J. Ellis, Protein folding: Importance of the Anfinsen cage. *Curr. Biol.* **13**, R881–R883 (2003).
27. A. C. Apetri, A. L. Horwich, Chaperonin chamber accelerates protein folding through passive action of preventing aggregation. *Proc. Natl. Acad. Sci. U.S.A.* **105**, 17351–17355 (2008).
28. A. L. Horwich, A. C. Apetri, W. A. Fenton, The GroEL/GroES cis cavity as a passive anti-aggregation device. *FEBS Lett.* **583**, 2654–2662 (2009).
29. J. C. Young, V. R. Agashe, K. Siegers, F. U. Hartl, Pathways of chaperone-mediated protein folding in the cytosol. *Nat. Rev. Mol. Cell Bio.* **5**, 781–791 (2004).
30. Y. C. Tang, H. C. Chang, A. Roeben, D. Wischnewski, N. Wischnewski, M. J. Kerner, F. U. Hartl, M. Hayer-Hartl, Structural features of the GroEL-GroES nano-cage required for rapid folding of encapsulated protein. *Cell* **125**, 903–914 (2006).
31. M. J. Avellaneda, E. J. Koers, D. P. Minde, V. Sunderlikova, S. J. Tans, Simultaneous sensing and imaging of individual biomolecular complexes enabled by modular DNA-protein coupling. *Commun. Chem.* **3**, 20 (2020).
32. M. J. Avellaneda, K. B. Franke, V. Sunderlikova, B. Bukau, A. Mogk, S. J. Tans, Processive extrusion of polypeptide loops by a Hsp100 disaggregase. *Nature* **74**, 317–320 (2020).
33. P. Bechtluft, R. G. H. van Leeuwen, M. Tyreman, D. Tomkiewicz, N. Nouwen, H. L. Tepper, A. J. M. Driessen, S. J. Tans, Direct observation of chaperone-induced changes in a protein folding pathway. *Science* **318**, 1458–1461 (2007).
34. A. Mashaghi, G. Kramer, P. Bechtluft, B. Zachmann-Brand, A. J. M. Driessen, B. Bukau, S. J. Tans, Reshaping of the conformational search of a protein by the chaperone trigger factor. *Nature* **500**, 98–101 (2013).
35. A. Mashaghi, S. Bezrukavnikov, D. P. Minde, A. S. Wentink, R. Kityk, B. Zachmann-Brand, M. P. Mayer, G. Kramer, B. Bukau, S. J. Tans, Alternative modes of client binding enable functional plasticity of Hsp70. *Nature* **539**, 448–451 (2016).
36. N. K. Tyagi, W. A. Fenton, A. A. Deniz, A. L. Horwich, Double mutant MBP refolds at same rate in free solution as inside the GroEL/GroES chaperonin chamber when aggregation in free solution is prevented. *FEBS Lett.* **585**, 1969–1972 (2011).
37. H. S. Rye, A. M. Roseman, S. Chen, K. Furtak, W. A. Fenton, H. R. Saibil, A. L. Horwich, GroEL-GroES cycling: ATP and nonnative polypeptide direct alternation of folding-active rings. *Cell* **97**, 325–338 (1999).
38. G. W. Farr, K. Furtak, M. B. Rowland, N. A. Ranson, H. R. Saibil, T. Kirchhausen, A. L. Horwich, Multivalent binding of nonnative substrate proteins by the chaperonin GroEL. *Cell* **100**, 561–573 (2000).
39. C. Cecconi, E. A. Shank, C. Bustamante, S. Marqusee, Direct observation of the three-state folding of a single protein molecule. *Science* **309**, 2057–2060 (2005).
40. J. Stigler, F. Ziegler, A. Gieseke, J. C. M. Gebhardt, M. Rief, The complex folding network of single-calmodulin molecules. *Science* **334**, 512–516 (2011).
41. M. M. Naqvi, P. O. Heidarsson, M. R. Otazo, A. Mossa, B. B. Kragelund, C. Cecconi, Single-molecule folding mechanisms of the apo- and Mg^{2+}-bound states of human neuronal calcium sensor-1. *Biophys. J.* **109**, 113–123 (2015).
42. K. A. Walther, F. Grater, L. Dougan, C. L. Badilla, B. J. Berne, J. M. Fernandez, Signatures of hydrophobic collapse in extended proteins captured with force spectroscopy. *Proc. Natl. Acad. Sci. U.S.A.* **104**, 7916–7921 (2007).
43. C. M. Dobson, A. Sali, M. Karplus, Protein folding: A perspective from theory and experiment. *Angew. Chem. Int. Ed. Engl.* **37**, 868–893 (1998).
44. S. Priya, S. K. Sharma, V. Sood, R. U. H. Mattoo, A. Finka, A. Azem, P. de Los Rios, P. Goloubinoff, GroEL and CCT are catalytic unfoldases mediating out-of-cage polypeptide refolding without ATP. *Proc. Natl. Acad. Sci. U.S.A.* **110**, 7199–7204 (2013).
45. J. Weaver, H. S. Rye, The C-terminal tails of the bacterial chaperonin GroEL stimulate protein folding by directly altering the conformation of a substrate protein. *J. Biol. Chem.* **289**, 23219–23232 (2014).
46. J. S. Weissman, C. M. Hohl, O. Kovalenko, Y. Kashi, S. Chen, K. Braig, H. R. Saibil, W. A. Fenton, A. L. Norwich, Mechanism of groel action: Productive release of polypeptide from a sequestered position under groes. *Cell* **83**, 577–587 (1995).
47. F. Motojima, M. Yoshida, Polypeptide in the chaperonin cage partly protrudes out and then folds inside or escapes outside. *EMBO J.* **29**, 4008–4019 (2010).
48. F. Motojima, M. Yoshida, Productive folding of a tethered protein in the chaperonin GroEL-GroES cage. *Biochem. Biophys. Res. Commun.* **466**, 72–75 (2015).
49. S. Sharma, K. Chakraborty, B. K. Müller, N. Astola, Y. C. Tang, D. C. Lamb, M. Hayer-Hartl, F. U. Hartl, Monitoring protein conformation along the pathway of chaperonin-assisted folding. *Cell* **133**, 142–153 (2008).
50. D. H. Chen, D. Madan, J. Weaver, Z. Lin, G. F. Schröder, W. Chiu, H. S. Rye, Visualizing GroEL/ES in the act of encapsulating a folding protein. *Cell* **153**, 1354–1365 (2013).
51. Z. Lin, H. S. Rye, Expansion and compression of a protein folding intermediate by GroEL. *Mol. Cell* **16**, 23–34 (2004).
52. J. L. England, V. S. Pande, Potential for modulation of the hydrophobic effect inside chaperonins. *Biophys. J.* **95**, 3391–3399 (2008).
53. N. Giovambattista, P. G. Debenedetti, P. J. Rossky, Effect of surface polarity on water contact angle and interfacial hydration structure. *J. Phys. Chem. B* **111**, 9581–9587 (2007).
54. H. S. Rye, Application of fluorescence resonance energy transfer to the GroEL-GroES chaperonin reaction. *Methods* **24**, 278–288 (2001).
55. K. Svoboda, S. M. Block, Biological applications of optical forces. *Annu. Rev. Biophys. Biom. Struct.* **23**, 247–285 (1994).
56. T. Odijk, Stiff chains and filaments under tension. *Macromolecules* **28**, 7016–7018 (1995).
57. I. M. Tolic-Norrelykke, K. Berg-Sorensen, H. Flyvbjerg, MatLab program for precision calibration of optical tweezers. *Comput. Phys. Commun.* **159**, 225–240 (2004).

Science Advances

Protein chain collapse modulation and folding stimulation by GroEL-ES

Mohsin M. NaqviMario J. AvellanedaAndrew RothEline J. KoersAntoine RolandVanda SunderlikovaGünter KramerHays S. RyeSander J. Tans

View the article online
https://www.science.org/doi/10.1126/sciadv.abl6293
Permissions
https://www.science.org/help/reprints-and-permissions

Use of this article is subject to the Terms of service